Materials and Methods

Preparation of graphene films

The starting material was 1-mm-thick platelets of highly-oriented pyrolytic graphite (HOPG). We used commercially available HOPG of grades ZYH (www.ntmdt.ru) and HOPG-1 (www.2spi.com) with μ >100,000 $cm^2/V \cdot s$ at 4K. Using dry etching in oxygen plasma (*S1*), we first prepared 5 μm-deep mesas on top of the platelets (mesas were squares of various sizes from 20 μm to 2 mm). The structured surface was then pressed against a 1-μm-thick layer of a fresh wet photoresist spun over a glass substrate. After baking, the mesas became attached to the photoresist layer, which allowed us to cleave them off the rest of the HOPG sample. Then, using scotch tape we started repeatedly peeling flakes of graphite off the mesas. Thin flakes left in the photoresist were released in acetone. When a Si wafer was dipped in the solution and then washed in plenty of water and propanol, some flakes became captured on the wafer's surface (as a substrate, we used n^+-doped Si with a SiO_2 layer on top; in order to avoid accidental damage - especially during plasma etching - we chose to use relatively thick SiO_2 with t =300nm). After this, we used ultrasound cleaning in propanol, which removed mostly thick flakes. Thin flakes (d < 10 nm) were found to attach strongly to SiO_2, presumably due to van der Waals and/or capillary forces.

To select from the resulting films only those that are just a few graphene layers thick, we used a combination of optical, electron-beam and atomic-force microscopy as described below. Graphitic films thinner than 50 nm are transparent to visible light but nevertheless can easily be seen on the SiO_2 surface because of the added optical path that shifts the interference colors. The color for a 300 nm wafer is violet-blue and the extra thickness due to graphitic films shifts it to blue. Fig. S1 shows our "color reference" that we use for estimates of films' thickness (one can find this photo useful for preparing similar films; be aware that shades of color may vary slightly for different microscopes). At thicknesses d less than $\approx$1.5nm, as measured by AFM, graphene films are no longer visible even via the interference shift as it becomes too small. This provides a natural marker that we use to distinguish between two groups of films that we refer to as few- and multi- layer graphene.

The graphene films whose properties are reported in the main paper were selected as those that were completely invisible in an optical microscope (OM). Although invisible in optics, few-layer graphene (FLG) can still be seen clearly in a high-resolution SEM (we used FEI Serion). To identify FLG films, we have compared optical and scanning-electron micrographs

of large areas on the wafer, trying to find the films visible in SEM but not in OM. To illustrate this approach, Fig. S2 shows a flake, which is easily identifiable on both SEM and optical images because of a thick region nearby. The FLG film gives a clear contrast in SEM but would be impossible to see in OM if an isolated FLG film were shown.

FLG films (selected as described above) were extensively studied by AFM (Multimode NanoScope III and AutoProbe M5), which in most cases gave readings for their *apparent* thickness d to be between 1 and 1.6 nm. The interlayer distance in bulk graphite is ≈3.35Å, which implies that FLG films were indeed only a few atomic layers thick. However, one should also take into account that at this level of resolution the apparent thickness measured by AFM includes the chemical and van der Waals contrasts (*S2*) (in our case, these lead to overestimating the actual thickness) and the distance between graphene and SiO_2, which is unknown even for atomically smooth surfaces and can be large (see below).

Single-layer graphene

AFM measurements have allowed us to identify many cases of single-layer graphene (SLG). Figs. 1C and S3 show examples of AFM images of single-graphene sheets. SLG was rarely found to lie completely flat, and we often observed some areas being ruptured and folded back (Fig. 1C) as well as "pleated" areas (Fig. S3, Right). For SLG, we measured the step heights of ≈4Å and 8Å for single and double folds, respectively. These values are in good agreement with the step height (d ≈4Å) measured for "nanographene" on top of HOPG (*S3*). This proves that such films were indeed single-layer graphene.

The AFM measurements on SLG also provide an estimate for the thickness of a "dead" layer between graphene and SiO_2. It varied from sample to sample and was typically several Å thick. Fig. S3 shows images for two extreme cases of small (d ≈5Å) and large (d ≈10Å) separation of graphene from SiO_2. d ≈5Å is consistent with expectations for an atomically smooth contact between graphene and SiO_2 surfaces (*S3*). However, films with d ≈5Å were found on rare occasions and only for graphene patches of rather small sizes ≤1μm^2. More commonly, we observed SLG with d up to ≈10Å. This can be attributed to the ever-present layer of absorbed water (*S4*), which remains captured between graphene and SiO_2. From the thickness of the "dead layer", we conclude that our FLG (identified as invisible in OM and having the *apparent* AFM thickness d ≈ 10 to 16Å) can contain only 1, 2 or maximum 3 layers of graphene. Finally, we note that single layer graphene was found among other FLG films rather frequently.

Microfabrication of graphene devices

After choosing FLG films as described above, we used electron-beam lithography to prepare resist masks of a desired geometry on top of the films. Then, we used dry etching in oxygen plasma to remove the graphitic material from everywhere but underneath the masks. The next step of lithography defined contact regions on top of the prepared mesas. This was followed by deposition of a 100nm Au (with a 5nm Cr underlayer) and the standard lift-off procedures (see Figs. 1 and S4).

For multilayer graphene, the resulting gold-to-graphene contacts had a typical resistivity of <50 Ω per μm of their length, roughly independent of d. For FLG, contact resistances were typically of about 1kΩ and varied strongly with gate voltage, in line with changes in resistivity ρ of FLG itself. In both cases, the contacts exhibited linear I-V characteristics without any evidence for the Schottky barrier down to nV biases. Finally, it should be noted that AFM tips were found to destroy FLG by peeling the films off the SiO_2 surface and then ripping them apart, or by scratching their surface. As scratches are detrimental for electrical continuity, we had to avoid the use of AFM for imaging of the films chosen for fabrication of the reported electronic devices. This so far did not allow us to identify the exact number of graphene layers (1, 2 or 3) in the studied devices.

Supporting Online Text

Model for the electric field effect in a 2D semimetal

With reference to Fig. S5, if the Fermi level ε_F lies between 0 and $\delta\varepsilon$, there are both electrons and holes present (the mixed state). In this case, the standard two-band model for a metal containing electrons and holes in concentrations n_e and n_h and with mobilities μ_e and μ_h describes its conductance σ by

$$\sigma = 1/\rho = e\cdot(n_e\mu_e + n_h\mu_h) \qquad (1)$$

and its Hall coefficient R_H by

$$R_H = (n_h\mu_h^2 - n_e\mu_e^2)/e\cdot(n_e\mu_e + n_h\mu_h)^2 \qquad (2)$$

Note that n_e and n_h are interdependent parameters related through a common value of ε_F.

If ε_F is shifted by electric-field doping below 0 (above $\delta\varepsilon$), only holes (electrons) are left and, instead of a semimetal, we get a completely hole (electron) conductor. Then, the metal's conductance is described simply by

$$\sigma = e \cdot n_{e,h} \cdot \mu_{e,h} \quad \text{and} \quad R_H = 1/en_{e,h} \qquad (3)$$

To calculate the dependence of σ and R_H on V_g for the whole range of gate voltages (such that ε_F varies from well below zero to well above $\delta\varepsilon$), we combined equations (1-3) with the equation for the induced (uncompensated) charge $n_h - n_e = n = e_0 e V_g/te$. Here we assume that at V_g =0 the semimetal is in the compensated state with equal concentrations of electrons and holes, $n_h = n_e = \frac{1}{2}n_0$. The results of our calculations for σ and R_H are shown in Figs. 2B,C while Fig. S6 shows the corresponding dependence for ρ (the latter is a 2D sheet resistivity given in Ohms per square).

Analysis of ShdH oscillations in few-layer graphene

Fig. S7 shows an example of our typical analysis of the observed ShdH oscillations in few- and multi- layer graphene. Although very time consuming, such analysis is most reliable and accurate, if there is a limited number of oscillations observed. Similar diagrams were plotted for every gate voltage to find B_F, the fundamental field that corresponds to ν =1.

The Fermi energy is given by equation $\varepsilon_F = \hbar eB_F/m$ (4), while the carrier concentration is $n = e_0 e V_g/te$ (5). Combining the two equations, one finds that the linear dependence $B_F \propto V_g$ (Fig. 3B) yields $\varepsilon_F \propto n$ and, hence, the constant density of states. As $\varepsilon_F \propto n^{2/D}$, where D is the dimensionality of an electronic system, the observed $B_F \propto V_g$ dependences prove unequivocally the 2D nature of charge carriers in few-layer graphene. The 3D dependence ($\varepsilon_F \propto n^{2/3}$) cannot possibly fit our experimental data (*S5*).

Fig. 3B shows that there is only one spatially quantized 2D subband occupied for the case of both hole and electron carriers. Indeed, if the second subband were to start populating at some gate voltages, this would result in a drastic change in slopes of the $B_F(V_g)$ curves (see below). The data in Figs. 3B, S8 and S9 prove that the second subband is not populated even for our highest carrier concentrations $\approx 3 \times 10^{13}$ cm^{-2}.

There are two types of holes in FLG, which is seen as two sets of ShdH frequencies for the same gate voltage in Fig. 3B. The ratio between their masses m_h^l/m_h^h (indices *h* and *l* refer to heavy and light holes, respectively) can be determined from these plots as follows (*S5*). If the gate voltage changes by dV_g, the Fermi energy has to shift by the equal amount $d\varepsilon_F$ for both

carriers. Therefore, equations (4-5) yield $(dB_F/dV_g)^l/m_h^l = (dB_F/dV_g)^h/m_h^h$, which shows that the ratio of slopes B_F/V_g yields the ratio between masses of heavy and light holes. In the case of FLG, we observe $m_h^h/m_h^l \approx 3.5$, in agreement with the values obtained from temperature dependences of ShdH oscillations (see the main text) (*S5*).

Furthermore, $B_F(V_g)$-curves prove that the carriers giving rise to the observed ShdH oscillations account for the whole electric charge n induced by gate voltage and, hence, there are no other, undetected carriers in graphene. Indeed, $n = mg\varepsilon_F/\pi\hbar^2 = (2e/h)\cdot gB_F$ where g is the valley degeneracy and factor 2 takes into account the spin degeneracy. The total concentration of holes induced by electric field doping is $n = n^h + n^l$, or $n = (2e/h)(g^hB_F^h + g^lB_F^l)$. The experimental data in Fig. 3B give $B_F^h = \alpha^hV_g$ and $B_F^l = \alpha^lV_g$ with $\alpha^l \approx 150$ mT/V and $\alpha^h \approx 570$ mT/V. On the other hand, equation (5) gives $n = \beta V_g$ where $\beta = 7.18\text{x}10^{10}$ cm^2/V. Combing the above expressions, we get the following numerical equation $\beta = (2e/h)(g^h\alpha^h + g^l\alpha^l)$ or $7.18\{1\%\} = 0.73\{4\%\}g^l + 2.76\{3\%\}g^h$, where {%} indicates the experimental accuracy of the numerical coefficients. As the valley degeneracy g has to be an integer number, the equation provides a unique solution with $g^l = g^h = 2$ (the numbers then match within the experimental accuracy). No other solution is possible.

For the case of electrons, there is only one set of ShdH oscillations with $\alpha \approx 740$ mT/V and, accordingly, we have another numerical equation $7.18\{1\%\} = 3.6\{3\%\}g$. This again yields $g = 2$. The observed double degeneracy of electrons and holes is in agreement with the theory of single-layer graphene.

2D electron and hole gases in multilayer graphene

In films thicker than ≈ 3nm, we observed charge carriers that are essentially different from those in FLG. Figs. S8 and S9 show examples of $B_F(V_g)$-curves for multilayer graphene. Although the electrons and holes induced by electric field doping are again strictly 2D (as the linear dependences of B_F on gate voltage show), now an additional type of electrons emerges. They are light ($m_e^l \approx 0.15m_0$) and have the quadrupole valley degeneracy ($g = 4$). All the other carriers are still double-valley degenerate. Moreover, the valence band also seems to change so that the ratio m_h^h/m_h^l becomes ≈ 6.5 (at least for the sample in Fig. S9), i.e. it is twice larger than in FLG. For thicker still films (typically, $d > 5$nm), we observed exactly the same 2D electrons and holes (e.g., compare Figs. S8 and S9). However, the thicker films also started exhibiting ShdH oscillations with frequencies independent of gate voltage (normally two

additional sets of ShdH oscillations). This indicates a contribution from layers that are unaffected by gate voltage and give the parallel conductance. The latter also results in a huge linear magnetoresistance typical for multilayer graphene. We believe that in multilayer graphene the 2D hole and electron gases induced by the field effect are located within a couple of nm near the SiO_2 interface (i.e. within several layers of graphene) while the rest of the material (next several graphene layers) remains unaffected, because electric field is efficiently screened by near-surface carriers.

I-V characteristics and doping of few-layer graphene

Fig. S10 shows typical I-V characteristics observed in our FLG devices at room temperature. I-V characteristics are found to be linear, and the devices could sustain extremely high current densities before they are destroyed at $\approx 1 mA/\mu m$, which is equivalent to $\geq 10^8 A/cm^2$ for nominal $d \approx 1nm$. There is some small non-linearity observed at high currents but this is attributed to self-heating, which leads to higher carrier concentrations at higher temperatures. Unlike in any other known transistor, gate voltage changes only slopes of I-V curves, i.e. its resistance R. Therefore, FLG devices could be called *field-effect variable resistors*. Fig. S11 illustrates that our devices can be doped by their exposure to various gases.

Supporting Figures and Legends

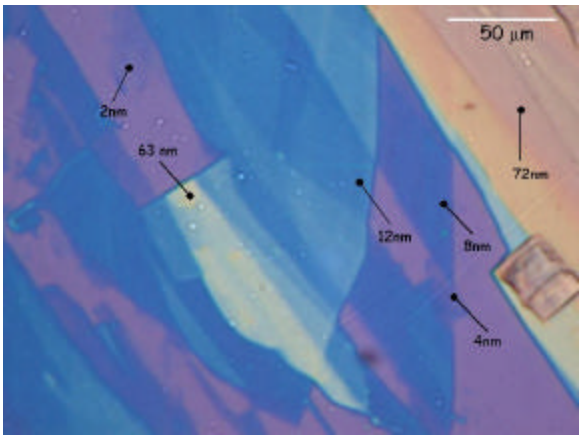

Figure S1. Optical photo in white light of graphitic films of various thickness *d*. The indicated values of *d* were measured by AFM. Note the area with $d \approx 2$ nm, which is barely visible in optics in the top-left corner.

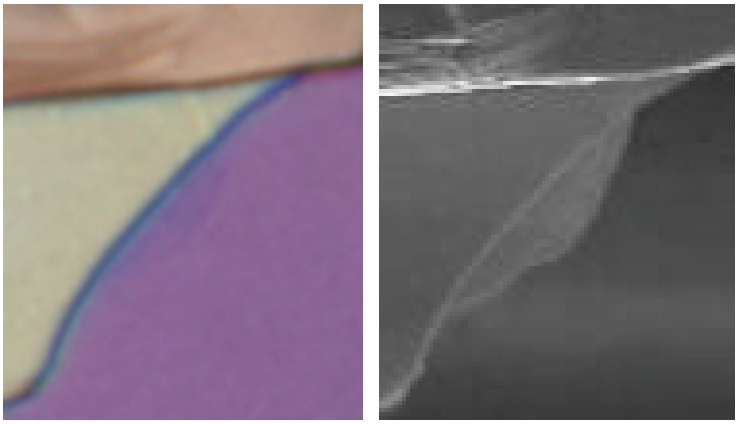

Figure S2. Images of a thin graphitic flake in optical (**Left**) and scanning electron (**Right**) microscopes. Few -layer graphene is clearly visible in SEM (in the center) but not in optics.

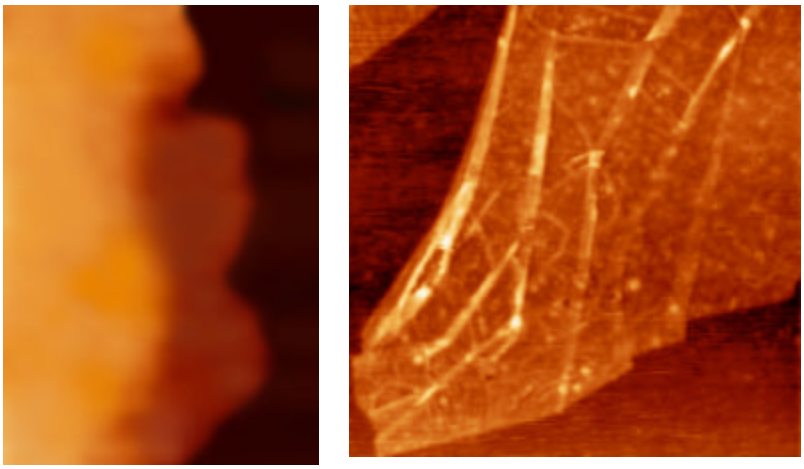

Figure S3. Single-layer graphene visualized by AFM. (**Left**) Narrow (≈100 nm) graphene stripe next to a thicker area. Colors: dark brown corresponds to SiO_2 surface, bright orange –2nm, light brown –0.5nm. (**Right**) SG sheet with several pleats (image size $3x3\mu m^2$). The thickness of double-folds is ≈8Å (the last fold on the right yields the value most precisely), proving that this is a single atomic sheet. Because of different interaction of an AFM tip with SiO_2 and graphene (tips were found to attract much stronger to SiO_2), only the contact AFM mode was generally found to give reliable readings of d, independent of

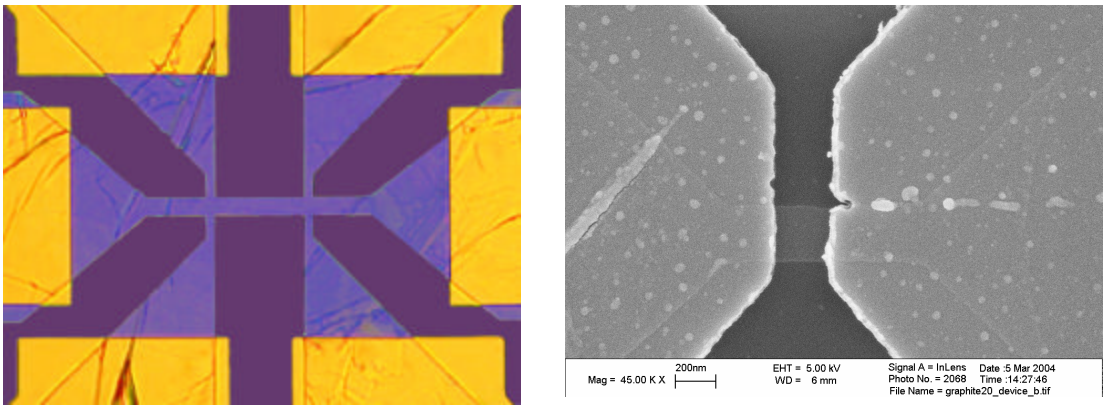

Figure S4. Additional images of our microfabricated devices. (**Left**) Optical photograph in white light of a large Hall bar made from multilayer graphene ($d \approx 5$nm). The central wire is 50μm long. (**Right**) A short (200 nm) wire made from few-layer graphene.

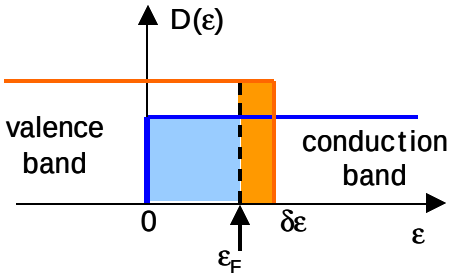

Figure S5. Schematic view of the density of states in a 2D semimetal used in our calculations.

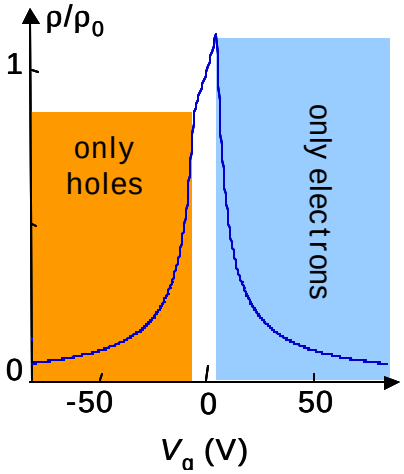

Figure S6. Calculated behaviour of ρ vs gate voltage. For simplicity, we assumed $\mu_e = \mu_h$. The asymmetry is due to different electron and hole masses ($m_h/m_e \approx 1.5$ as found from ShdH measurements).

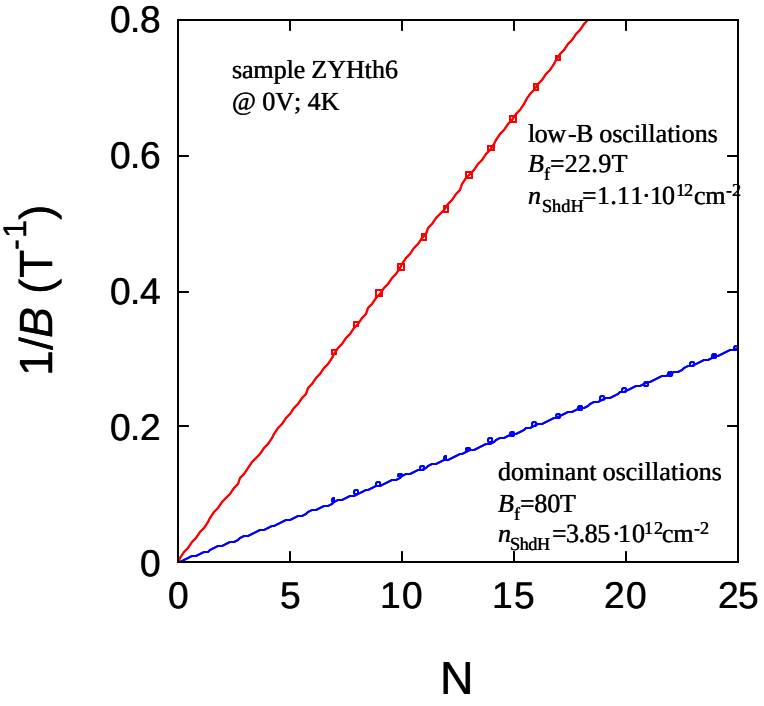

Figure S7. Standard fan diagrams used in our analysis of ShdH oscillations. *N* is the number associated to different minima or maxima in the oscillations. Only two sets of frequencies were found in this sample for all gate voltages. Values of B_F yield effective carrier concentrations $n_{ShdH} = (2e/h)B_F$.

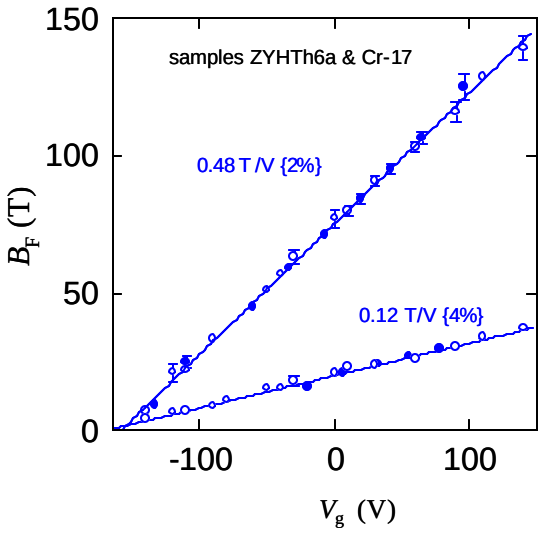

Figure S8. $B_F(V_g)$-curves for two samples of multilayer graphene. Symbols are experimental data obtained from the analysis of ShdH oscillations as explained in Fig. S7. Solid lines are best fits (% in brackets is the accuracy of defining the experimental slopes).

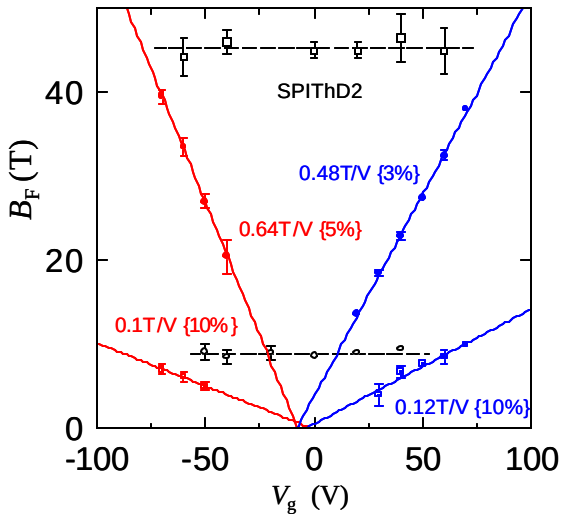

Figure S9. Another multilayer sample, where also additional ShdH oscillations independent on gate voltage (with $B_F \approx 9$ and 45T) are clearly seen. Note that the slopes of $B_F(V_g)$-curves for electrons are the same as in Fig. S8.

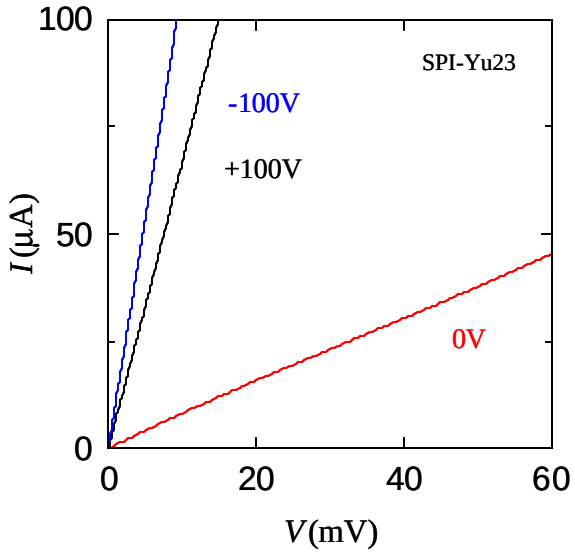

Figure S10. I-V characteristics of an FLG device of 0.5μm width for three different gate voltages (4-probe geometry).

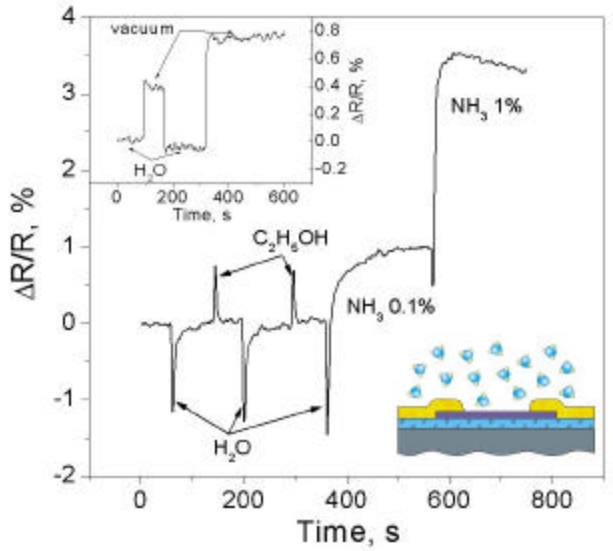

Figure S11. Four-probe resistance R of a relatively thick multilayer device (d≈5nm) during its exposure to various gases. A few-seconds exposure to clean nitrogen with 0.1% of water rapidly reduces R that later recovers to the original state. Similar behavior is observed for ethanol but changes in R are positive (n-doping). Ammonia is also a donor but changes in R become permanent indicating stronger binding between NH_3 and graphene. It requires heating up to ≈200C to recover the original state. The inset shows that there is a permanent layer of water absorbed on graphene surfaces, which can be removed – at least partly – by placing samples in vacuum.

Supporting References and Notes

S1. X. Lu, H. Huang, N. Nemchuk, R.S. Ruoff, *Appl. Phys. Lett.* **75**, 193 (1999).

S2. M. Guggisberg *et al*, *Phys. Rev.* B **61**, 11151 (2000).

S3. K. Harigaya, Y. Kobayashi, K. Takai, J. Ravier, T. Enoki, *J. Phys. Cond. Mat.* **14**, L605 (2002).

S4. J.N. Israelachvili, *Intermolecular and Surface Forces* (Academic, London 1991).

S5. Note that the linear dispersion spectrum theoretically expected for graphene also yields the observed dependence $B_F \propto V_g$, similar to the 2D free-electron model used in the paper. It is beyond the scope of this work to discuss the meaning of the effective masses obtained via the standard procedure of fitting the temperature dependence of ShdH oscillations for the case of the linear dispersion.

S6. We thank the anonymous referee of our Science manuscript for pointing out that a linear dispersion spectrum should result in a density of states proportional to their energy.